AUT Journal of Electrical Engineering

AUT J. Elec. Eng., 55(2) (2023) 305-320
DOI: 10.22060/eej.2023.22202.5521

A Plasmonic Refractive Index Sensor Using a Water-Based Metamaterial Absorber

S. Zamani Noughabi[1], A. S. Nooramin[2]*, M. Soleimani[3]

Department of Electrical Engineering, The Iran University of Science and Technology (IUST), Tehran. Iran

ABSTRACT: A structure for refractive index sensing application in THz band is proposed and analyzed in this paper. This structure is comprised of a golden plasmonic metamaterial absorber in which water is used as a dielectric and a thin TOPAS layer-which does not have a significant effect on the performance of the sensor- is used for the separation of analyte and water. This structure has an absorption of 99.2% at resonance frequency of 2.8725 THz. Lateral absorption frequency shift occurs due to variation in the refractive index (RI) of the analyte. This structure can be used for refractive index measurement in the range of 1-1.4 with full-width half maximum (FWHM), sensitivity (S), the figure of merit (FoM), and quality factor (Q-factor) in the ranges of 0.01647 THz, 427-644 GHz per refractive index unit (RIU), 6.3-26.5 and 26.23-175.5, respectively. It is worth mentioning that for a limited refractive index range of 1.1 to 1.15, the values of FWHM, Q-factor, and FoM enhance to 0.0053327 THz, 516, and 90, respectively. The simplicity, compactness, and ease of fabrication due to the use of water as a dielectric along with appropriate refractive index sensitivity and FoM help this structure to be used in biological, medical, and environment sensing applications.

Review History:

Received: Feb. 14, 2023
Revised: Apr. 28, 2023
Accepted: May, 23, 2023
Available Online: Oct. 01, 2023

Keywords:

Absorber
metamaterial
sensor
plasmonic

1- Introduction

Today, many efforts have been devoted to making terahertz technology usable in the real world. Among them, medical applications in the detection of cells and tissue have been expanded using sensors. In most of them, the analysis is done by measuring the refractive index (RI) in the range of 1-1.5 in the liquid phase i. e. analyte [1]–[2].

To this end, many types of sensors have been proposed. Among them, metamaterial absorber sensors attract a lot of attention today. These are sub-wavelength periodic structures in which artificially designed to display a negative refractive index. Sensors based on metamaterial absorbers are very attractive due to their high sensitivity (S) and figure of merit (FoM) [3]–[5]. Enhanced sensing performance achieves if surface plasmon polaritons (SPPs) can be excited in this kind of sensor. SPPs are coherent electron oscillations that propagate along metal-dielectric or metal-air interface. The excitation of SPPs will result in the concentration of electric field in the metal-dielectric interface and consequently making an increment in absorption at the resonance frequency and the quality factor (Q-factor) of the structure [6].

Generally, many kinds of dielectric are used in this kind of sensor. Beyond them, water-based sensors attract much attention due to their ease of fabrication, cheapness, and compatibility with the environment. Actually, in this structure, the variety of used materials is limited to water and gold [7,8].

In this paper, a water-based metamaterial plasmonic absorber sensor is presented, which is used to measure the RI of analytes in the range of [1-1.4]. the values of full-width half maximum (FWHM), Q-factor, sensitivity, and FoM in the range of 0.01647 THz, 26.23-175.5, 427-644 GHz per refractive index unit (RIU), and 6.3-26.5 along with the simplicity of the proposed structure present the superior sensing performance of the sensor compared to others. A detailed evaluation of the structure along with its results will be given below.

2- Sensor Design And Simulation Result

The unit cell of the proposed metamaterial sensor is presented in Fig. 1. As shown in Fig. 1(a), this structure is composed of a golden substrate that is emptied into a rectangular cubic and filled with water. At the center of this structure, a golden cylinder is placed.

This cylinder has the main role in exciting surface plasmons at the operating frequency which is desirable for achieving the highest sensitivity of the sensor. All the dimensions of the structure are given in Table 1. This structure is terminated in a short circuit as shown in Fig 1(a).

*Corresponding author's email: A_nooramin@iust.ac.ir

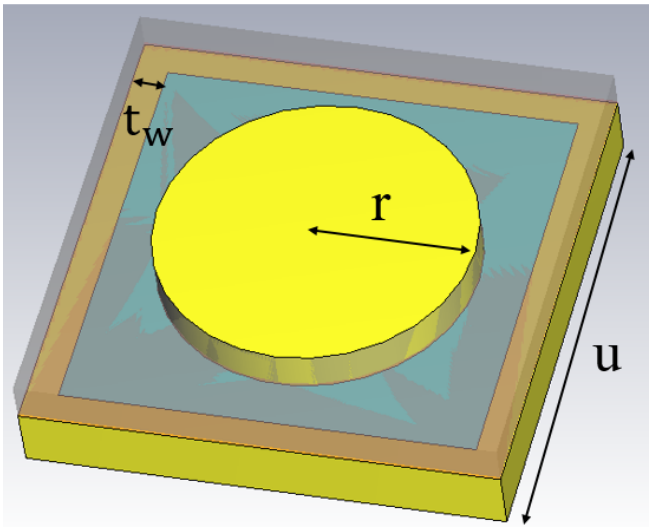

(a)

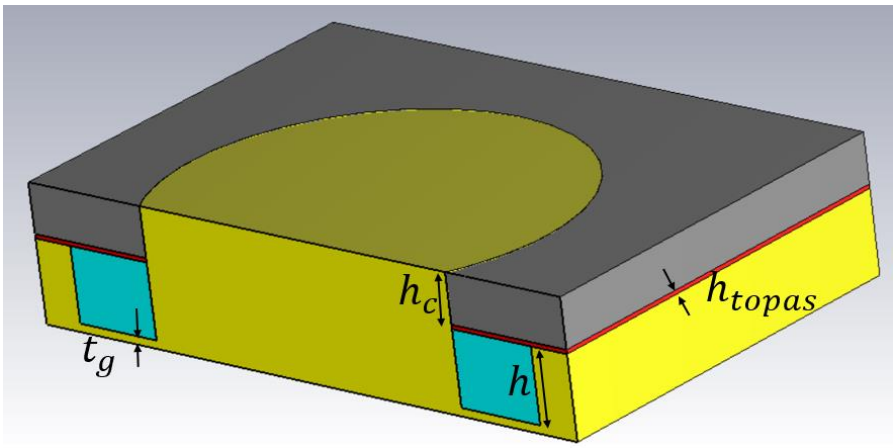

(b)

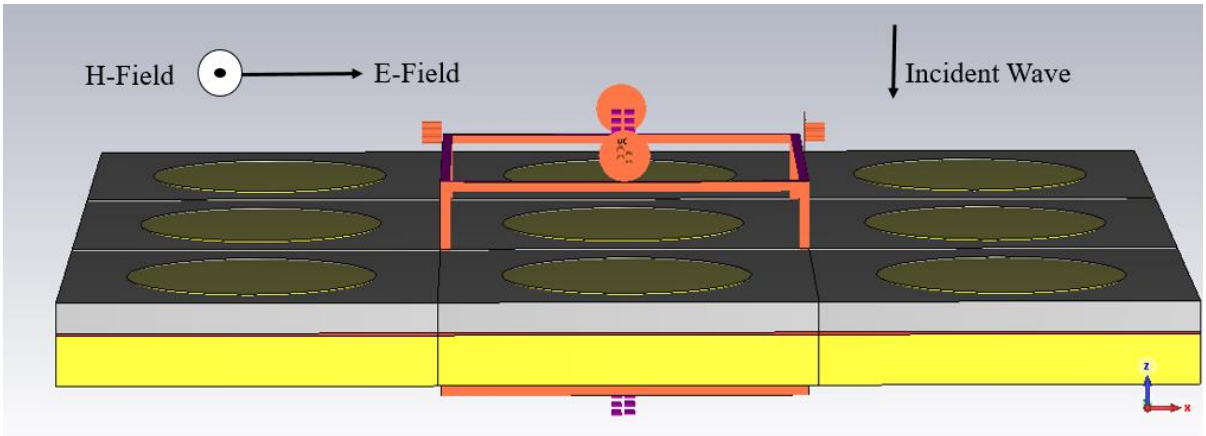

(c)

Fig. 1. Sensor unit cell (a) top view. (b) Cutaway side view. (c) An overview of the metamaterial absorber and related cross section and incident wave direction.

Table 1. The Parameter Of The Structure And Their Values

Parameter	Value	Unit
u	150	μm
h	*18*	μm
h_c	12	μm
r	50	μm
t_w	10	μm
t_g	2	μm
h_{topas}	1	μm
ε_∞(gold)	5.9673	F/m
ω_p(gold)	1.328×10^{16}	rad/s
γ(gold)	5.7805×10^{13}	1/s
ε(water)	4	F/m
tanδ(water)	0.5	
ε(topas)	2.343	F/m
tanδ(TOPAS)	0.007	

F = farad, rad = radian, s = second

As shown in Fig. 1(b), a TOPAS layer is placed on the substrate to separate the water from the analyte and it has no effect on the sensing performance, as shown later. Actually, the analyte is poured on the TOPAS and it will be the same height as the cylinder. The values of epsilon and loss tangent of TOPAS according to [14] are also given in Table 1 and permittivity and loss tangent of TOPAS layer in different wavelengths are shown in Fig. 2. An overview of the material absorber is shown in Fig. 1(c).

In the analysis of structure, the Drude model is used for describing the conductivity of gold at THz band, according to (1) [6].

$$\varepsilon(\omega)=\varepsilon_\infty-\omega_p^2/(\omega^2+i\omega\gamma) \quad (1)$$

Refer to (1), ε_∞ is the high-frequency dielectric constant, ω_p is the plasma frequency, ω is the angular frequency, and γ is the damping constant [6]. The values of these parameters for gold at THz are shown in Table 1 according to [13].

Furthermore, the values of relative permittivity and the loss tangent of water at THz frequencies are used in the analysis as mentioned in Table 1 [7], [12].

In this paper, Numerical simulation is done using CST Microwave Studio software, and floquet periodic boundary conditions are applied in the x and y directions to imitate the infinite periodicity of the sensor. The incident TEM plane wave toward the z-direction is simulated by using a flouqet port in software, as shown in Fig. 1(c), and the S- parameter is calculated.

The amount of absorption at each frequency is calculated according to:

$$A=1-T-R=1-|S_{21}|^2-|S_{11}|^2 \quad (2)$$

where T and R stand for the transmission and reflection coefficients, and are equal to values of $|S_{21}|^2$ and $|S_{11}|^2$ in the software, respectively. The thickness of the bottom layer t_g is chosen such that the value of the transmission coefficient becomes equal to zero.

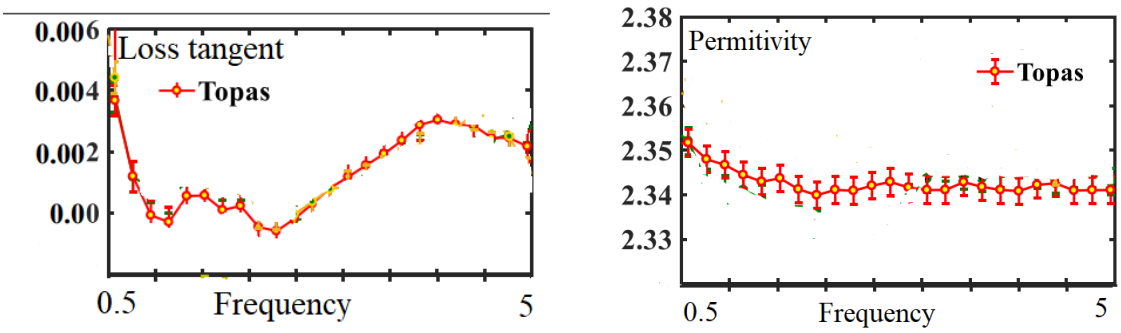

Fig. 2. Permittivity and loss tangent of TOPAS for different frequencies [14].

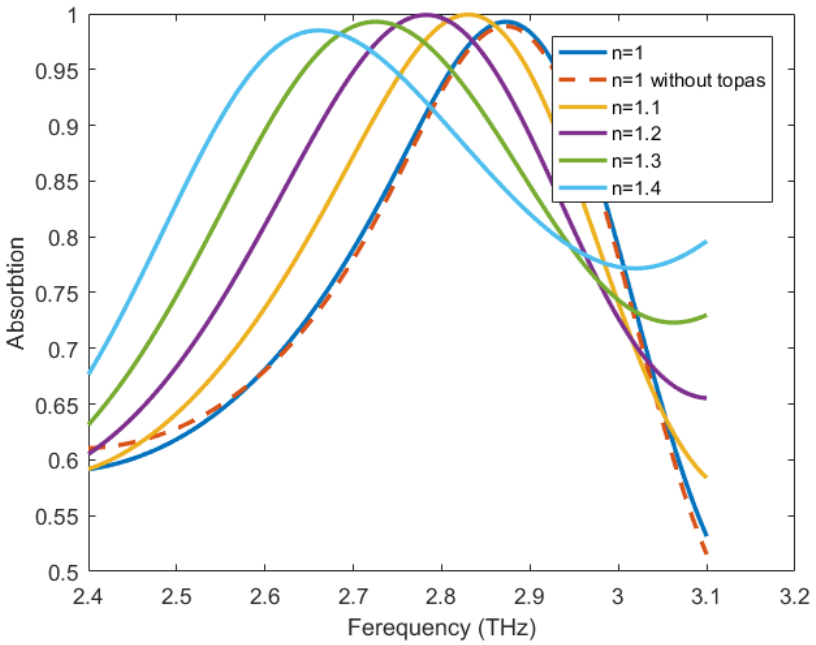

Fig. 3. Absorption spectrum for various refractive indices of analyte.

The absorption of the structure for different analytes has been analyzed and shown in Fig. 3. In this analysis, the refractive index (n) of the analyte is assumed to be real in the range of [1-1.4].

Furthermore, the values of the absorption peak remain around one for the mentioned refractive index. Therefore, this sensor can be used for refractive index measurement, as explained in the next section.

The frequency of absorption peak versus refractive index is plotted in Fig. 4. It is shown clearly in this figure that these values of frequencies decrease monotonically with increasing refractive index with a slope of approximately 528.75 GHz/ RIU .

The dependence of the absorption on the changes in the height of a cylinder (h_c), height of water (h), radius of cylinder (r), thickness of the golden wall (t_w), unit cell dimensions (u), and height of TOPAS (h_{Topas}) are examined in Fig. 5. In these analyses, it is assumed that n = 1.1.

As depicted in Fig. 5(a), the value and frequency of the absorption peak decrease slightly by increasing the height of the golden cylinder (h_c). Similarly, a decrement in water height (h) results in a small reduction in the frequency and the value of the absorption peak, as shown in Fig. 5(b). The analysis for the dependency of absorption on the radius of the golden cylinder reveals that the absorption characteristics remain constant with little variation in radius (r), as shown in Fig. 5(c).

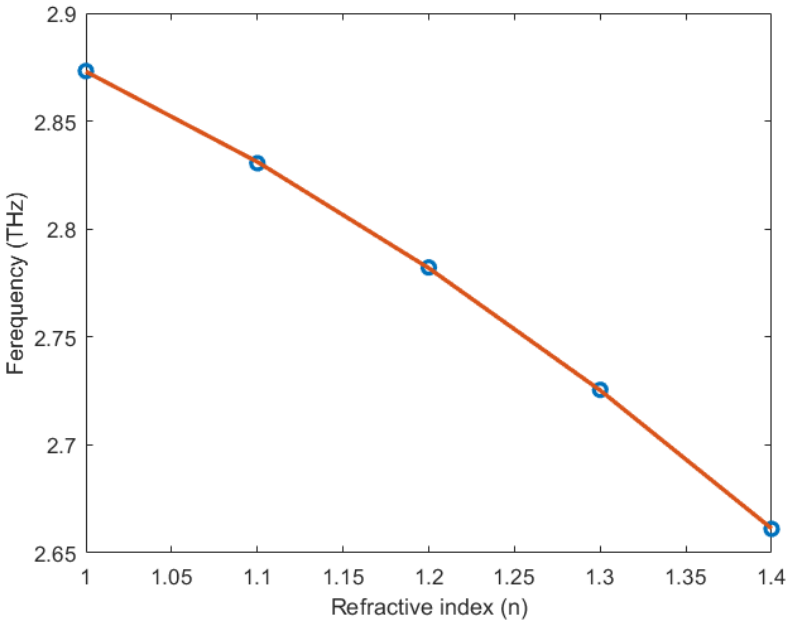

Fig. 4. The frequency of absorption peak versus refractive index.

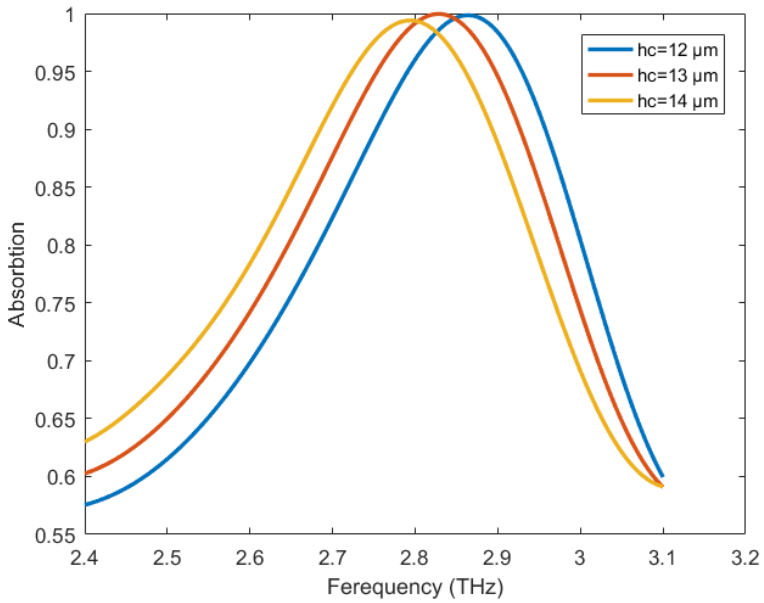

(a)

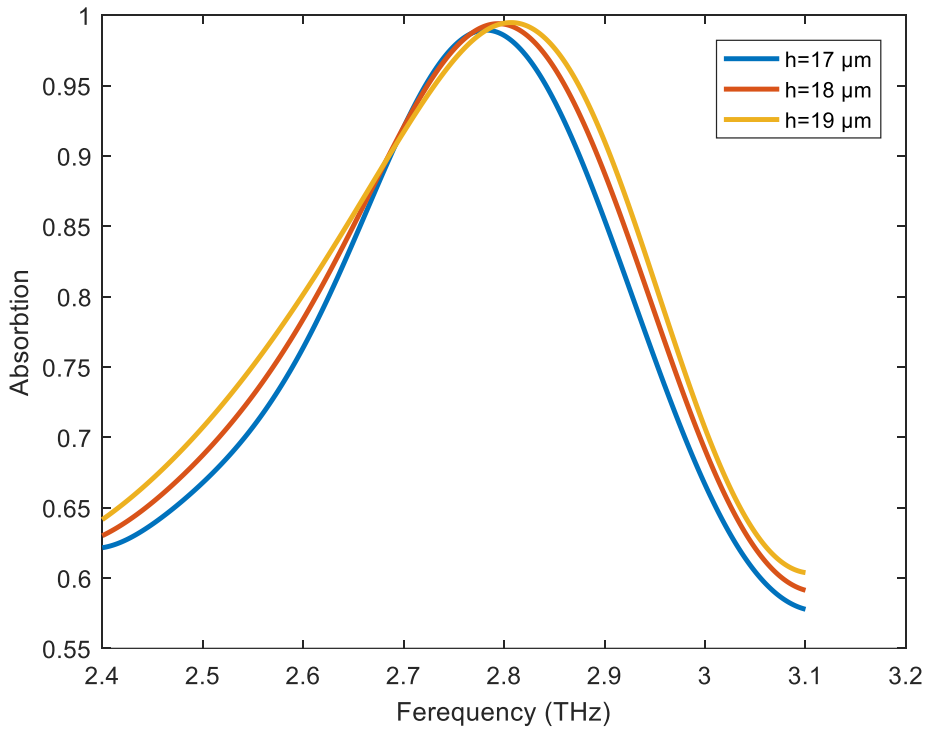
h=17 μm
h=18 μm
h=19 μm
Absorbtion
Ferequency (THz)
1
0.95
0.9
0.85
0.8
0.75
0.7
0.65
0.6
0.55
2.4
2.5
2.6
2.7
2.8
2.9
3
3.1
3.2

(b)

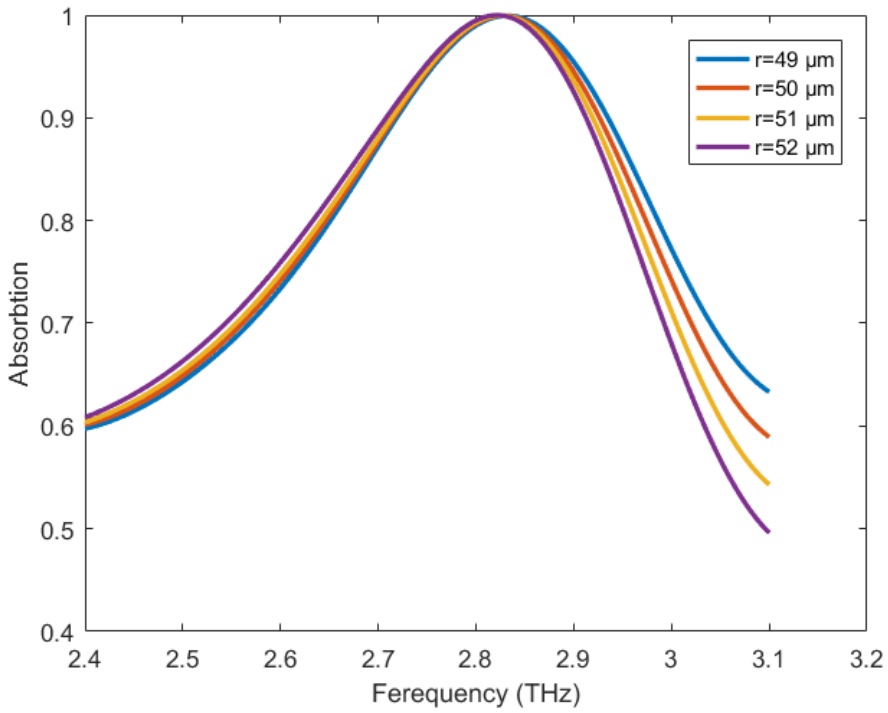
r=49 μm
r=50 μm
r=51 μm
r=52 μm
Absorbtion
Ferequency (THz)
1
0.9
0.8
0.7
0.6
0.5
0.4
2.4
2.5
2.6
2.7
2.8
2.9
3
3.1
3.2

(c)

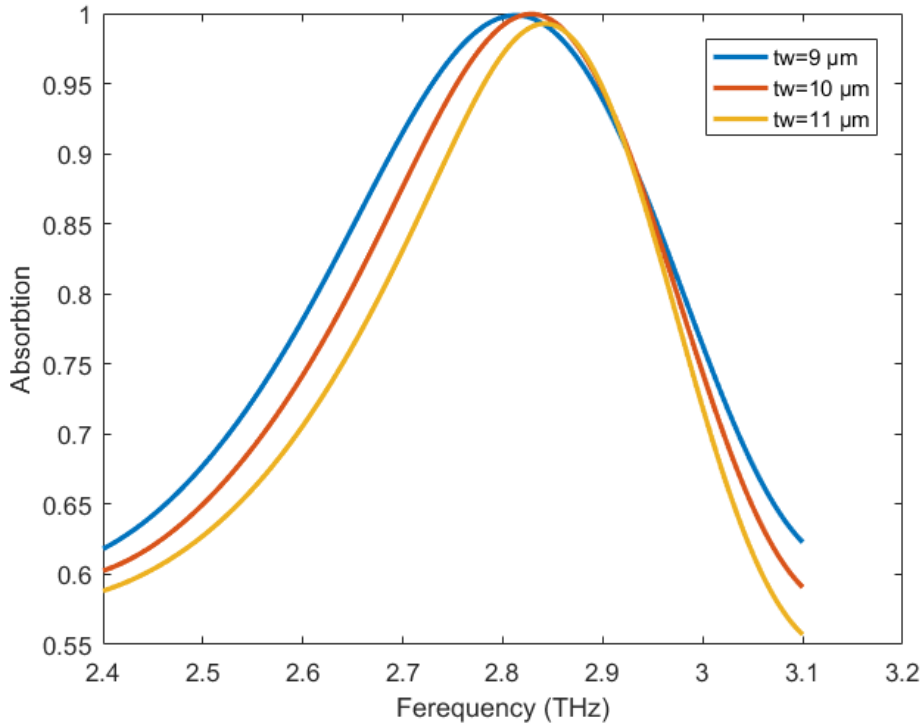
tw=9 μm
tw=10 μm
tw=11 μm
Absorbtion
Ferequency (THz)
1
0.95
0.9
0.85
0.8
0.75
0.7
0.65
0.6
0.55
2.4
2.5
2.6
2.7
2.8
2.9
3
3.1
3.2

(d)

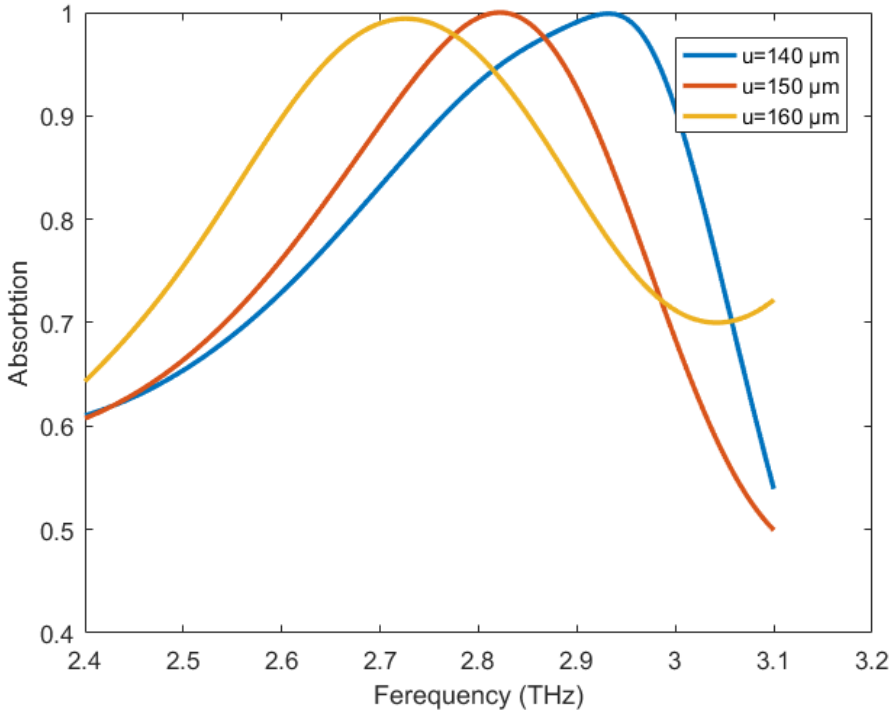
u=140 μm
u=150 μm
u=160 μm
Absorbtion
Ferequency (THz)
1
0.9
0.8
0.7
0.6
0.5
0.4
2.4
2.5
2.6
2.7
2.8
2.9
3
3.1
3.2

(e)

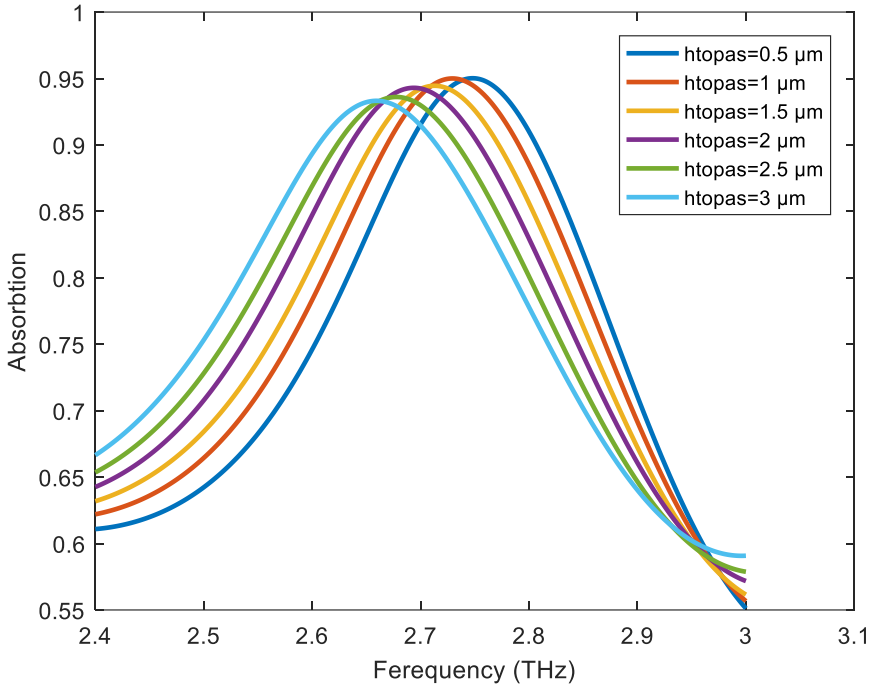

(f)

Fig. 5. Parametric analysis of the proposed structure. (a) Golden cylinder height (hc). (b) Water height (h). (c) The radius of the golden cylinder (r). (d) Wall thickness (tw) and (e) Unit cell dimension (u). (f) topas layer (htopas)

Making an increment in the thickness of the golden wall (t_w), results in an enhancement in the frequency of the absorption peak while that value remains constant, As depicted in Fig. 5(d). Likewise, any changes in the periodicity of the structure (u) cause to shift in the frequency of the absorption peak, whereas the absorption peak value remains constant, as shown in Fig. 5(e). Lower resonance frequencies are related to structures with higher TOPAS thickness, as shown in Fig. 5(f).

In Fig. 6, the absorption spectrum is plotted for different values of polarization angle of the incoming wave. Since the structure is symmetrical, a polarization-insensitive nature is expected, as evident in Fig. 5.

3- Analysis of Simulation Result

In this section, the performance of the structure has been analyzed. For this and at the first step, the behavior of the structure against the incident plane wave will be evaluated. As shown in Fig. 7, the plane wave that radiates vertically from top to bottom on the structure forms a standing wave by the reflected wave from the structure. In this figure, the intensity of the electric field is shown in the cross-section of the structure for (a) 0°, (b) 30º, (c) 45º, (d) 90º, and (e) 150º phase angles.

For both TE and TM incident waves and due to the high conductivity of the gold, we have:

$$\overrightarrow{E_t} = 0 \tag{3}$$

Where $\overrightarrow{\boldsymbol{E}_t}$ stands for the tangential component of the electric field on the structure. Therefore, the standing wave maxima will be located at the following distances relative to the surface,

$$d = n\frac{\lambda_{inc}}{2}.n = 1.3.5.\ldots \tag{4}$$

A deeper look at Fig. 7 shows that there is a break in the wavefront of the incoming wave and in the place between the two cylinders. A transverse standing wave is also created between the two cylinders. The electric fields of this standing wave are spread into the water and its maximum is located between the two cylinders. The approximate resonance wavelength for this wave will be obtained as follows,

$$\lambda_{res} \approx m(u - 2r).m = 1.2.3.\ldots \tag{5}$$

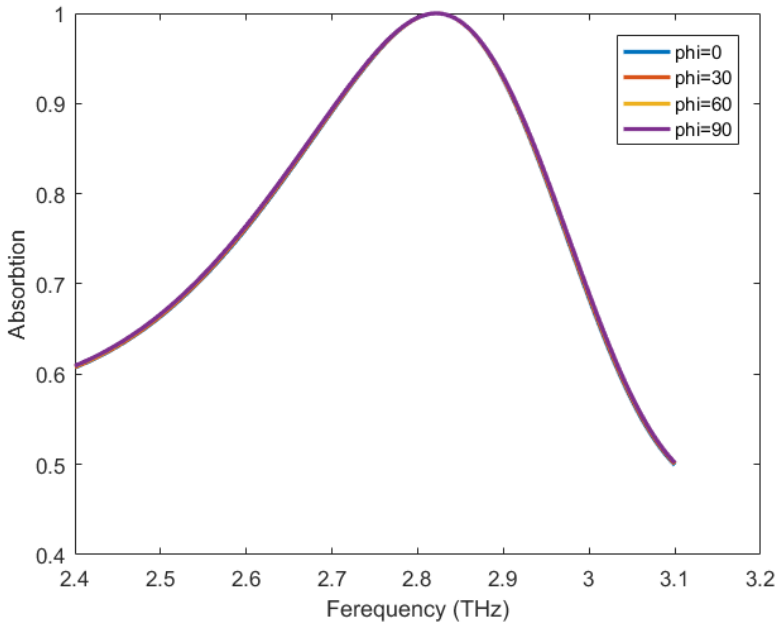

Fig. 6. Absorption diagram polarization angle of the incident incoming wave.

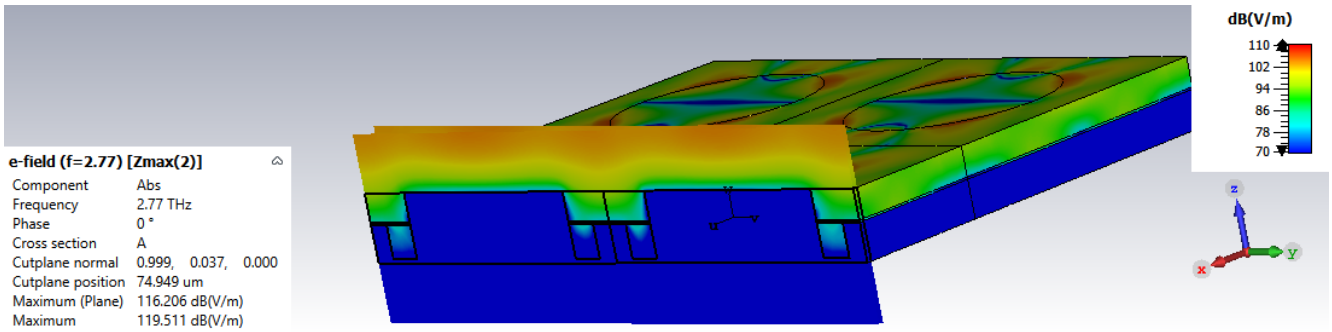

(a)

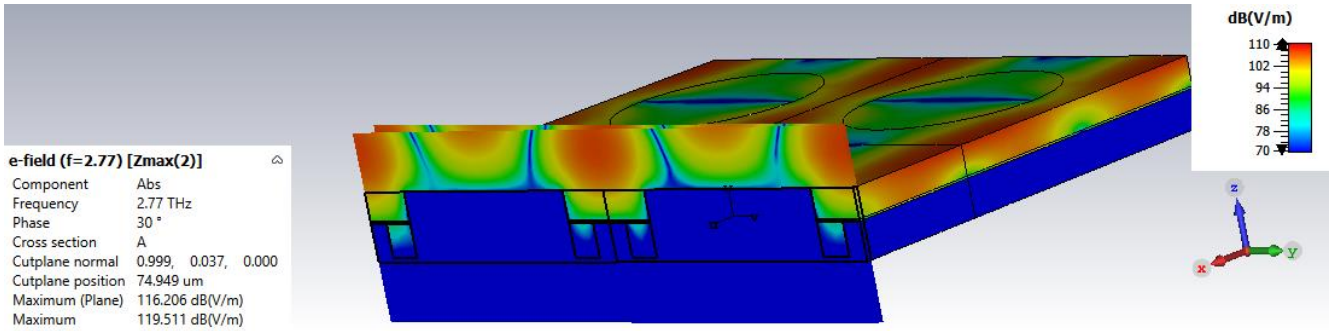

(b)

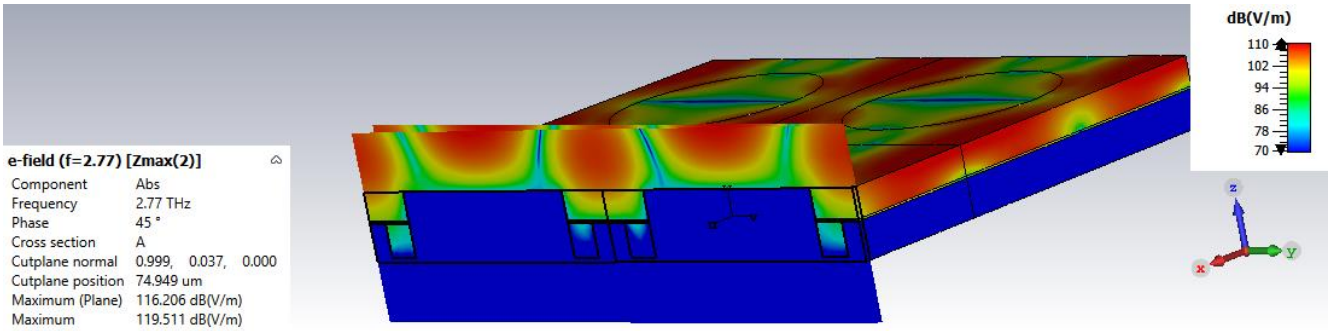

(c)

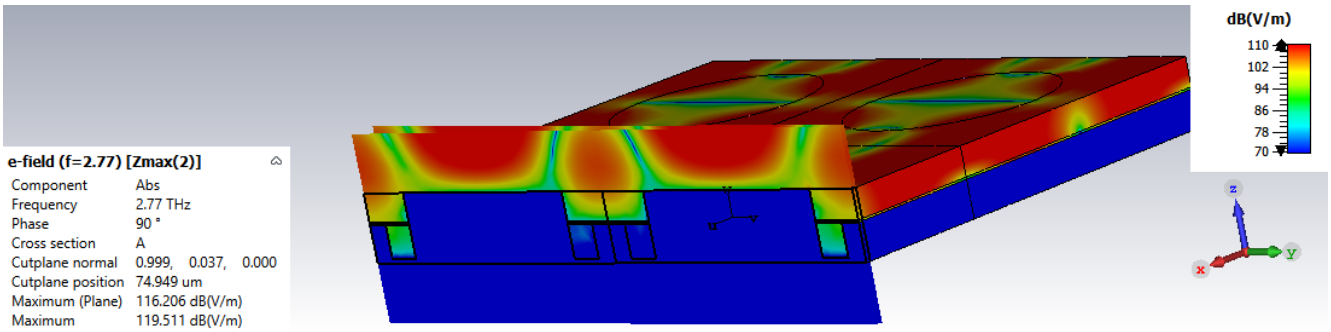

(d)

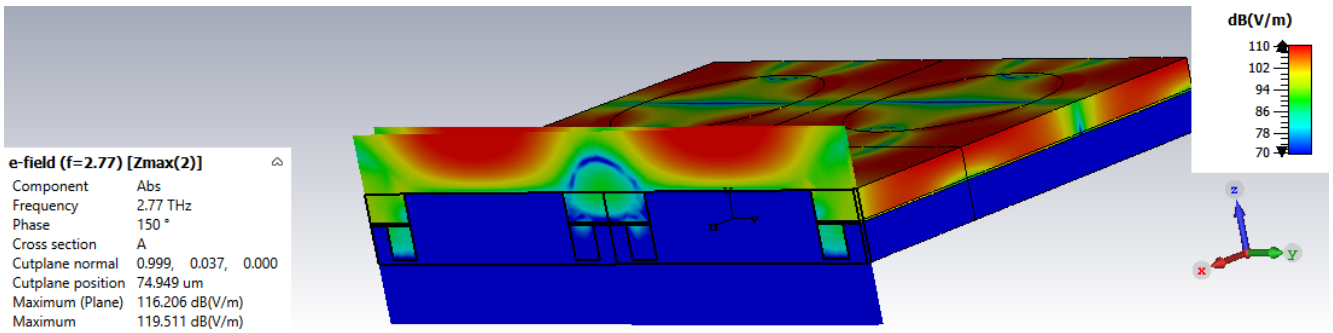

(e)

Fig 7. The Intensity of the E-Field in cross section for (a) 0°, (b) 30°, (c) 45°, (d) 90°, and (e) 150°.

For the values presented in the proposed structure, $(u-2r)=100\mu m$ while $\lambda_{res}=108\mu m$.. Therefore, the description of the transverse standing wave is reasonably accurate. The difference in wavelength is due to different values of distance between two cylinders in their cross sections. Based on this assumption, the resonance frequency should be independent of the height of the cylinder and highly depend on the h_c , t_w , and u , as shown in Fig. 5.

The absorption spectrum of the structure, when the entire space between the two cylinders inside the structure is filled with the analyte, is shown in Fig. 9. As shown in this figure, the lower resonance frequency corresponds to the higher refractive index of the analyte. In fact, with the increase of the refractive index, the wavelength decreases, and according to equation (5), we can expect a decrease in the resonance frequency. Furthermore, the peak of the absorption spectrum

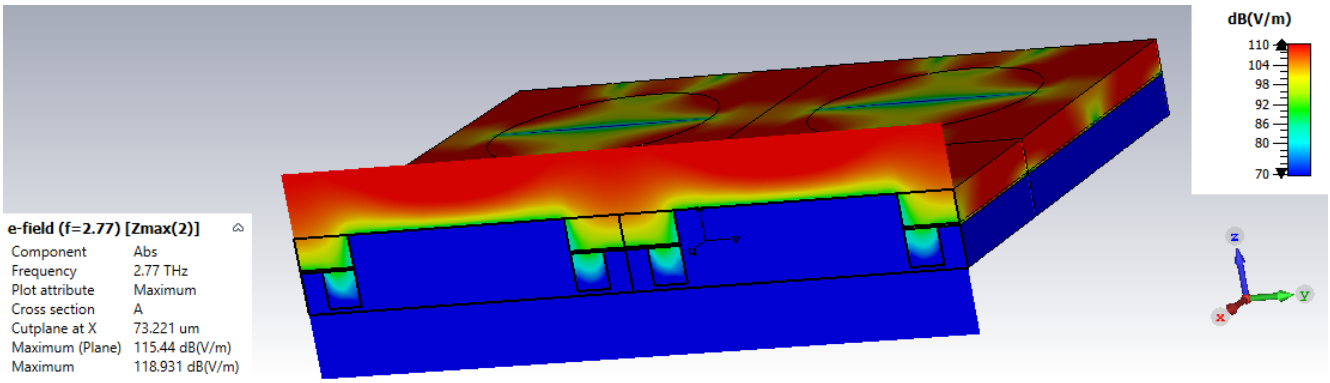

(a)

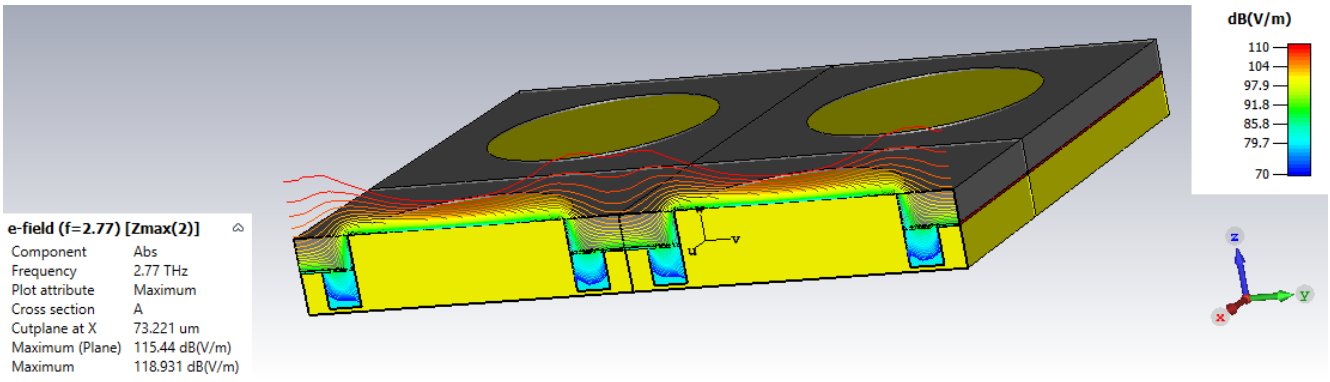

(b)

Fig 8. Maximum E-Field in cross-section. (a).Contour of E-Field and (b). Isolines of E-Field.

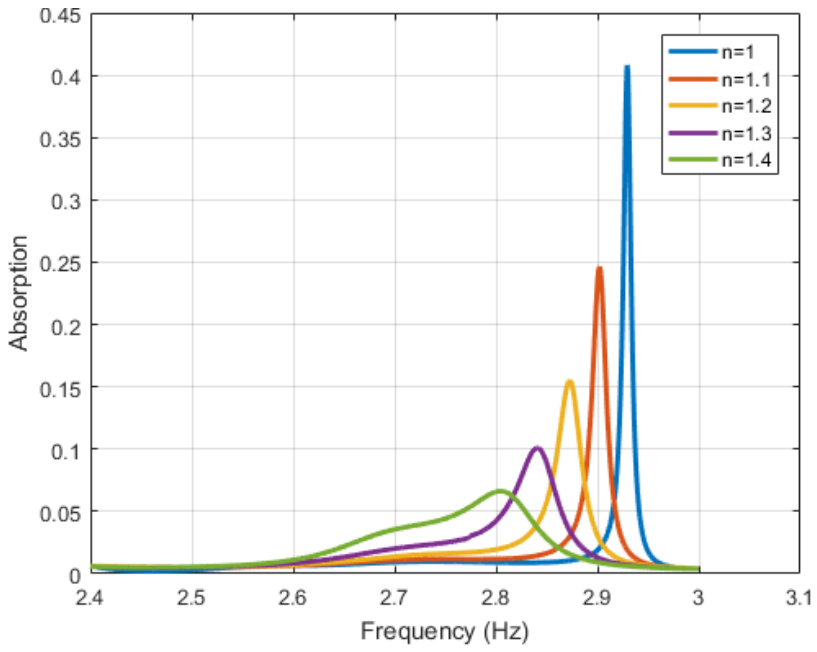

Fig 9. Absorption spectrum for the structure which is filled with analyte by various refractive index.

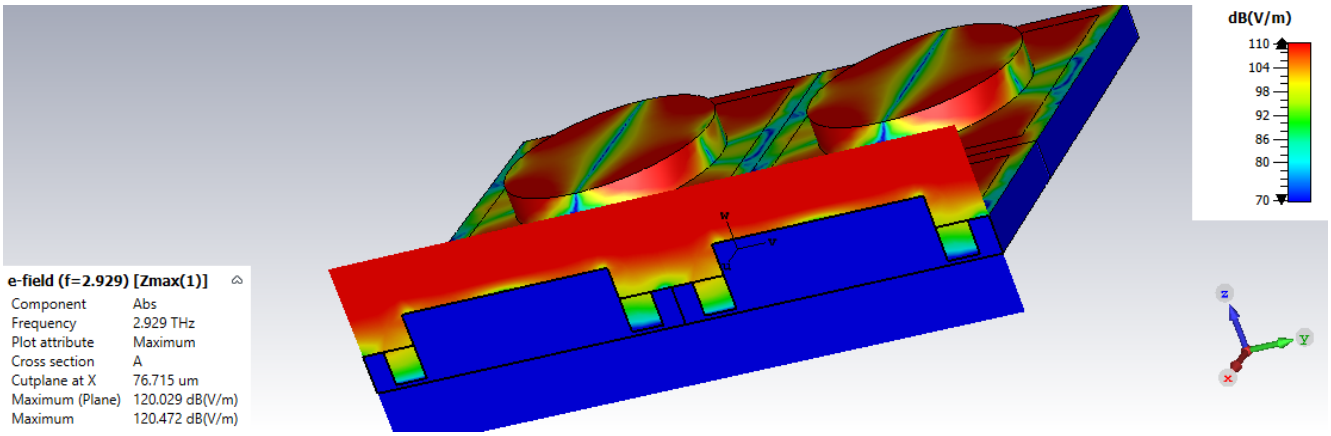

Fig 10. The intensity of E-Field distribution in the cross section of the structure without water. In this figure, the whole structure is filled with the analyte by n=1.

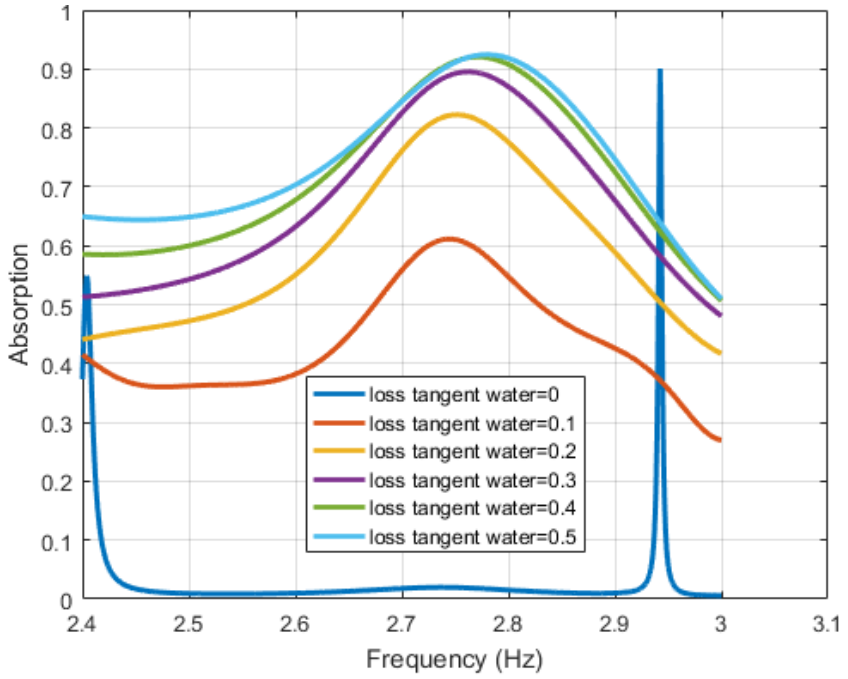

Fig 11. Absorption spectrum for water that difference loss tangent.

for higher values of the refractive index decreases. A close look at Figure 9 shows that with the increase of the refractive index, another resonance mode is being formed around the frequency of 2.7 THz, which will cause the reduction of the resonance quality factor. Also, due to the lower refractive index of the analyte compared to water, the maximum standing field in the structure without water is located above the level of the analyte, and as a result, the sensor sensitivity will decrease. It is shown clearly in Fig. 10. In this figure, the intensity of the electric field in the cross-section of the structure is shown for the structure which is filled by the analyte of $\boldsymbol{n}=1$. By comparing Fig. 9 and Fig. 3, it can be seen that the sensor with the presence of water has a more suitable performance for the range of analyte refractive index [1-1.4].

Further study of the role of water in sensor performance has been done and shown in Fig. 11. In this figure, the absorption spectrum of the structure is plotted for different values of water loss tangent in the structure without analyte. As shown in Fig.11, by the increment of the water loss tangent coefficient, the absorption of the structure increases. In fact, as we expected, the water loss coefficient modifies the curve of the absorption spectrum of the structure. The highest Q-factor belongs to the zero loss tangent coefficient.

4- Sensing Performance Analysis

In this section, the goal is to evaluate the performance of the proposed sensor. For this and at the first step, the basic parameters used in all sensing applications are introduced and discussed.

The first one is the Q-factor which is the ratio of resonant frequency to FWHM, as given in the following equation:

$$Q = f_0 / FWHM \tag{6}$$

The lower value of FWHM is important in sensing applications because it improves the sensitivity due to the small spectral width. Therefore, higher values of quality factors are desirable. The value of the FWHM for the sensor is about 0.05925 THz at 2.8725 THz, which indicates the high sensitivity of the sensor. Furthermore, the characteristics of the quality factor versus refractive index are plotted in Fig. 12(b). According to this figure, the value of the quality factor improves with the increase of the refractive index, while its value is always more than 26.

Another important parameter in sensing applications is sensitivity which is defined as a ratio of the resonance frequency variation to the refractive index variation of the analyte, as

$$S = \Delta f_0 / \Delta n \tag{7}$$

In Fig. 12(a), the values of sensitivity are plotted versus refractive index. $S > 390$ for the range of refractive index [1-1.4] is achieved which can be reached up to 600 for the $n > 1.25\ \Delta n \leq 0.1$. This feature makes the sensor preferable in sensing applications.

Another important criterion is called figure of metric (FoM) which is defined as the ratio of the sensitivity to the FWHM of the sensor as

$$FoM = S / FWHM \tag{8}$$

Since the lower values of FWHM are desirable, a sensor with the larger values of FoM is more valuable in sensing applications. FoM of the proposed sensor is depicted in Fig. 12(c) as a function of the refractive index. As explained above, $FoM > 9$ the refractive index range of [1-1.4] and values above 30 for $1.1 < n < 1.15\ \Delta n \leq 0.1$ have been achieved.

Table 2 presents a comparison between the achieved results and previous works.

According to the presented results in this Table 2, the proposed structure shows better sensing performance compared to other structures. It should be mentioned that in some report, low frequency values of conductivity are used for metals. Since metal conductivity decreases at THz band, the quality factor and as a result the sensing performance of these sensors degrade.

Table 2. Comparison Between The Performed Works

Reference	Range of refractive index	S (GHz/RIU)	Q-factor	FoM
[3]	1 – 1.39	300	22.05	2.94
[17]	1 – 1.8	163	–	2.67
[18]	1 – 1.6	851	13.76	–
[19]	–	532	–	–
[9]	1 – 2.5	96.2	–	7.8
[10]	1.333 – 1.464	23.08	–	–
[15]	1.3 – 1.4	1447	92.75	36.175
[11]	–	187	32.167	6.015
[5]	1.3 – 1.36	1600	225	80
[16]	1 – 2	126	44.17	10.5
This work	1 – 1.4	427–644	26.23–175.5	6.3–26.5

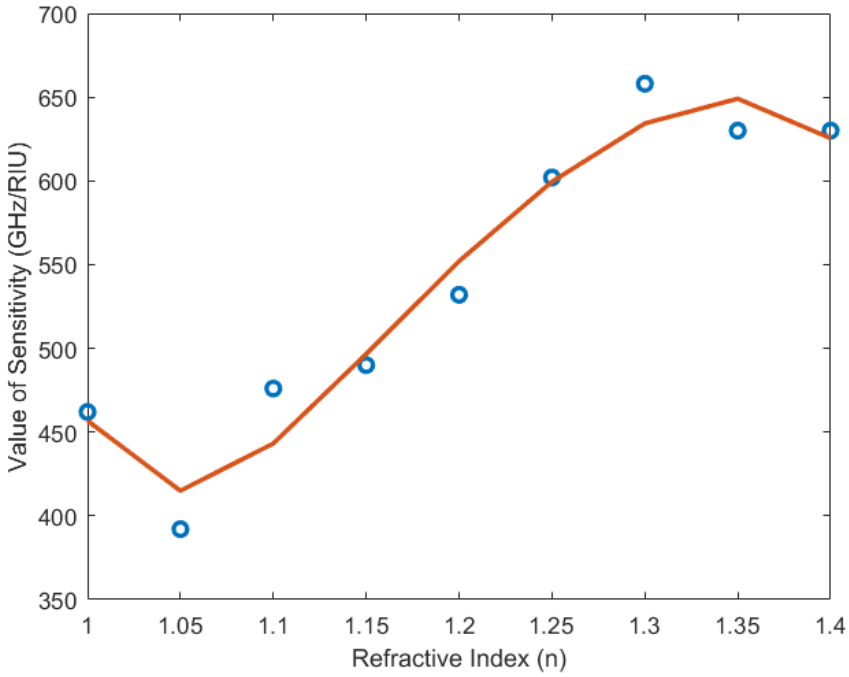

(a)

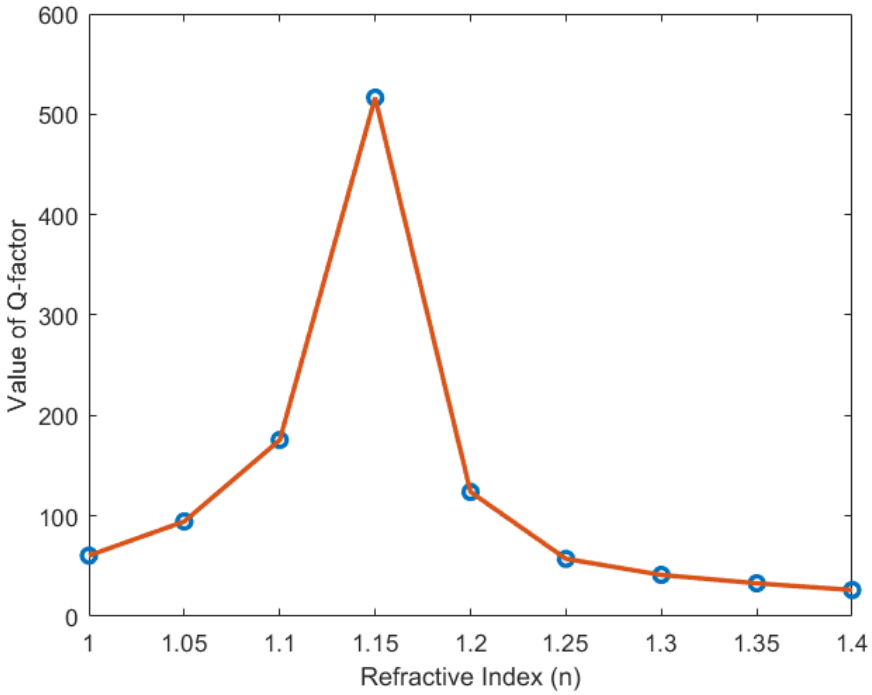

(b)

Fig. 12. (a) Sensitivity, (b) Q-Factor, and (c) FoM for the proposed.

5- Conclusion

In this paper, a structure for the water-based plasmonic metamaterial sensor is introduced. This structure is composed of a golden frame that is filled with water, as a dielectric. A TOPAS layer is used due to the isolation of water from the analyte. The absorption band shifts laterally if the refractive index of the analyte changes. Due to the symmetry of the structure, the polarization-insensitive nature of the sensor is also found. The proposed sensor offers up to 99% absorption at the frequency range of 2.66-2.87 THz due to a refractive index of [1-1.4]. Furthermore, a minimum FWHM of 0.01647 THz, resulting in a high Q-factor of 175.5, and the possibility of increasing the quality factor up to 516 for a limited refractive index range of [1.1-1.15] are the other advantages of the proposed sensor. In the same way, the sensor sensitivity and FoM are calculated to be 644 GHz/RIU and 26.5 which can be enhanced to 658 GHz/RIU and 90, respectively. Higher Q-factor, FoM, and sensitivity in addition to the simplicity of the structure make this structure as a suitable choice in biomedical sensing applications.

References

[1] F. Chen, Y. Cheng, and H. Luo, "Temperature Tunable Narrow-Band Terahertz Metasurface Absorber Based on InSb Micro-Cylinder Arrays for Enhanced Sensing Application, " IEEE Access, vol. 8, pp. 82981-82988, 2020

[2] M. Y. Azab, M. F. O. Hameed, A. M. Nasr and S. S. A. Obayya, "Highly Sensitive Metamaterial Biosensor for Cancer Early Detection, " IEEE Sensors Journal, vol. 21, no. 6, pp. 7748-7755, March. 2021.

[3] A. S. Saadeldin, M. F. O. Hameed, EM. A. Elkaramany, and SS. A.Obayya, "Highly Sensitive Terahertz Metamaterial Sensor," IEEE Sensor Journal, vol. 19, no.18, pp. 7993-7999, Sept. 2019.

[4] F. Li, K. He, T. Tang, Y. Mao, R. Wang, C. Li, and j. Shen, "The terahertz metamaterials for sensitive biosensors in the detection of ethanol solutions," Opt. Communications, vol. 475, Nov. 2020.

[5] A. Mohanty, O. P. Acharya, B. Appasani, S. K. Mohapatra, and M. S. Khan, "Design of a Novel Terahertz Metamaterial Absorber for Sensing Applications," IEEE Sensor Journal, vol. 21, no.20, pp. 22688-22694, Oct. 2021.

[6] M. Askari, "A near infrared plasmonic perfect absorber as a sensor for hemoglobin concentration detection," Opt Quant Electron, vol. 53, 2021.

[7] Z. Vafapour, W. Troy, and A. Rashidi, "Colon Cancer Detection by Designing and Analytical Evaluation of a Water-based THz Metamaterial Perfect Absorber," IEEE Sensor Journal, vol. 21, no. 17, pp. 19307–19313, Sept. 2021.

[8] Z. Vafapour et al, "The potential of Refractive Index Nanobiosensing using a Multi-band Optically Tuned Perfect Light Metamaterial Absorber," IEEE Sensor Journal, vol. 21, no. 12, pp. 13786–13793, Jun. 2021.

[9] W. Pan, Y. Yan, Y. Ma, and D. Shen, "A Terahertz Metamaterial Based on Electromagnetically Induced Transparency Effect and its Sensing Performance," Opt. Communications, vol. 431, pp. 115–119, Jan. 2019.

[10] Y. Wang, W. Cheng, J. Qin, and Z. Han, "Terahertz refractive index sensor based on the guided resonance in a photonic crystal slab," Opt. Communications, vol. 434, pp. 163–166, 2019.

[11] S. Banerjee et al, "A Terahertz Metamaterial Absorber Based Refractive Index Sensor with High Quality Factor, " 2021 13th International Conference on Electronics, Computers and Artificial Intelligence (ECAI), 2021, pp. 1-4.

[12] M. Hishida, and K. Tanaka, "Transition of the hydration state of a surfactant accompanying structural transitions of self-assembled aggregates," J Phys Condens Matter, vol. 24, no. 28, Jul. 2012.

[13] H. Hsiao, A. Abass, J. Fischer, R. Alaee, A. Wickberg, M. Wegener, and C. Rockstuhl, "Enhancement of second-harmonic generation in nonlinear nanolaminate metamaterials by nanophotonic resonances," Opt. Express, vol. 24, 2016.

[14] MD. Saiful Islam et al, "Experimental Study on Glass and Polymers: Determining the Optimal Material for Potential Use in Terahertz Technology," IEEE Sensor Journal, vol. 8, pp. 97204–97214, 2020.

[15] S. Banerjee, P. Dutta, A. V. Jha, B. Appasani, and M. S. Khan, "A Biomedical Sensor for Detection of Cancer Cells Based on Terahertz Metamaterial Absorber," IEEE Sensor Letters, vol. 6, no. 6, pp. 1–4, June. 2022.

[16] Z. Xiong et al, "Terahertz Sensor With Resonance Enhancement Based on Square Split-Ring Resonators," IEEE Access, vol. 9, pp. 59211–59221, 2021.

[17] L. Cong, and R. Singh, "Sensing with THz metamaterial absorbers," physics.optics, Aug. 2014.

[18] MR. Nickpay, M. Danaie, and A. Shahzadi, "Highly Sensitive THz Refractive Index Sensor Based on Folded SplitRing Metamaterial Graphene Resonators," Plasmonics, vol. 17, pp. 237–248, 2022.

[19] H. M. Silalahi, YP. Chen, Y. Shin, YS. Chen, X. Lin, J. Liu, and C. Huang, "Floating terahertz metamaterials with extremely large refractive index sensitivities," Photon. Res, vol. 9, pp. 1970–1978, 2021.

[20] S. Banerjee, U. Nath, P. Dutta, A. V. Jha, B. Appasani, and N. Bizon, "A Theoretical Terahertz Metamaterial Absorber Structure with a High Quality Factor Using Two Circular Ring Resonators for Biomedical Sensing," Inventions, vol. 6, no. 4, pp. 78, 2021

HOW TO CITE THIS ARTICLE

S. Zamani Noughabi, A. S. Nooramin, M. Soleimani, A Plasmonic Refractive Index Sensor Using a Water-Ba -sed Metamaterial Absorber, AUT J. Elec. Eng., 55(2) (2023) 305-320.

DOI: 10.22060/eej.2023.22202.5521